Dynamic Function-Structure Connectivity Coupling for Predicting Progression Trajectories in Neurocognitive Decline

Qianqian Wang[1], Wei Wang[2], Hong-Jun Li[2], Weili Lin[1], Mingxia Liu[1,*]

[1] Department of Radiology and BRIC, University of North Carolina at Chapel Hill, Chapel Hill, North Carolina 27599, USA
[2] Department of Radiology, Beijing Youan Hospital, Capital Medical University, Beijing, China
*Corresponding author (mingxia_liu@med.unc.edu)

Abstract. Function-structure connectivity (FSC) coupling helps reveal alterations in the interplay between brain functional connectivity (FC) and structural connectivity (SC) caused by neurocognitive decline. Existing studies on FSC coupling typically focus on modeling interactions between static FC and SC features, ignoring temporal dynamics conveyed in functional MRI (fMRI) time series. Additionally, conventional strategies often compute global whole-brain FSC correlation or assess local region-specific FSC correspondences, without capturing complex inter-region dependencies between FC and SC patterns. To this end, we propose a dynamic function-structure connectivity coupling (DFSC) framework to predict progression trajectories in neurocognitive decline with fMRI and diffusion tensor imaging (DTI) data. In DFSC, we first construct static SC and dynamic FC graphs and use graph neural networks (GNNs) for feature learning, yielding new SC and FC embeddings. Based on these embeddings, we construct *dynamic local-to-global FSC coupling graphs* to capture both *region-specific and inter-region dependencies* between FC and SC, followed by GNNs to generate dynamic FSC coupling embeddings. These multi-view embeddings are finally fed into a squeeze-excitation readout module and a Transformer for feature fusion and prediction. Experimental results on two datasets with paired fMRI and DTI data from a total of 231 subjects demonstrate that our DFSC outperforms several state-of-the-art methods. With the DFSC, one can identify both discriminative brain regions and between-group FSC coupling difference, facilitating objective quantification of structural and functional brain changes associated with neurocognitive decline.

Keywords: Dynamic function-structure coupling · Neurocognitive decline · Functional MRI · Diffusion tensor imaging

1 Introduction

Resting-state functional MRI (fMRI) reflects brain neural activity fluctuations by detecting blood oxygenation level-dependent signals, while diffusion tensor

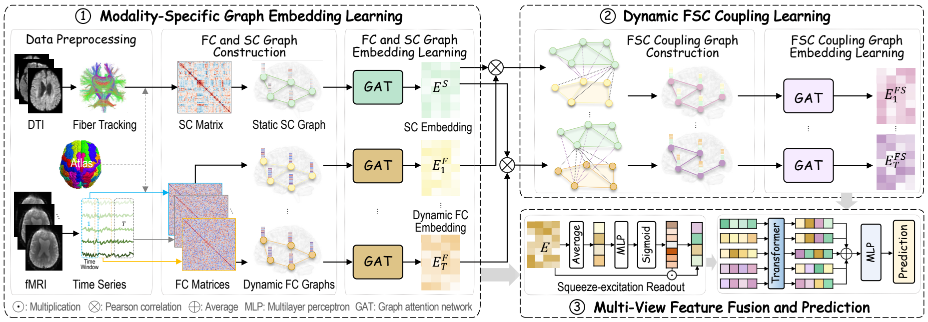

Fig. 1. Illustration of the proposed DFSC framework, consisting of (1) modality-specific graph embedding learning from fMRI and DTI data, (2) dynamic function-structure connectivity (FSC) coupling learning, and (3) multi-view feature fusion and prediction.

imaging (DTI) reveals brain anatomical structure by quantifying white matter tracts [8]. Function-structure connectivity (FSC) coupling analysis provides insights into alterations in the interplay between brain functional connectivity (FC) derived from fMRI and structural connectivity (SC) from DTI, facilitating detection of neurocognitive decline [2,5,27]. However, previous FSC coupling studies generally focus on investigating interactions between static FC and SC patterns, without considering dynamic properties of FC that fluctuate over time [21].

Additionally, existing studies often model whole-brain FSC coupling by computing correlation coefficients between vectorized FC and SC features, suggesting that FSC coupling alteration is associated with cognitive decline [20]. However, they ignore regional-level FSC coupling changes, limiting their ability to detect fine-grained imaging biomarkers. Some recent efforts have been devoted to characterizing local correspondences of paired regions in FC and SC networks [14,26], but fail to capture inter-region dependencies between FC and SC patterns.

To this end, we propose a dynamic function-structure connectivity coupling (DFSC) framework to predict progression trajectories in neurocognitive decline with fMRI and DTI. As shown in Fig. 1, we first construct static SC and dynamic FC graphs and use graph neural networks (GNNs) for modality-specific graph embedding learning, generating new SC and FC features respectively. By measuring correlation strength across all regions between each of multiple dynamic FC embeddings and the static SC embedding, we construct *dynamic local-to-global FSC coupling graphs* to capture both *region-specific and inter-region dependencies* between FC and SC, followed by GNNs to learn dynamic FSC coupling features. After that, a squeeze-excitation readout converts these multi-view graph embeddings into graph-level feature vectors. Finally, a Transformer is applied to integrate multi-view features (*i.e.*, FC, SC, and FSC), followed by a multi-layer perceptron (MLP) for prediction. Experiments on two datasets with paired resting-state fMRI and DTI data from a total of 231 subjects demonstrate the superiority of DFSC. With DFSC, one can identify both discriminative brain regions and between-group FSC coupling difference, enhancing objective quantification of brain functional and structural changes associated with neurocognitive decline. To our knowledge, this is among the first attempts to model temporally dynamic FSC coupling graphs while capturing local-to-global regional interactions between FC and SC patterns derived from fMRI and DTI data.

2 Materials and Methodology

2.1 Subjects and Data Preprocessing

Two datasets are included: a public ADNI [18] dataset and an in-house dataset (called HCD) [31]. The ADNI contains 46 subjects with subjective memory complaints (SMC) with paired fMRI and DTI data and 48 gender- and age-matched normal controls (NCs). The HCD includes 68 HIV-infected patients who exhibit asymptomatic neurocognitive impairment (ANI) and 69 NCs.

The fMRI data are preprocessed using DPARSF [34], including discarding the first 10 volumes for magnetization equilibrium, slice-timing correction, head motion correction, nuisance signal regression, co-registration with T1-weighted MRI, spatial normalization to MNI space, bandpass filtering (0.01–0.10 Hz), and extracting the average time series of 116 regions-of-interest (ROIs) defined by AAL atlas. The DTI data are preprocessed using PANDA [6]: head motion correction, eddy current correction, skull removal, registration with T1-weighted MRI, and fiber tracking. With AAL, we can generate a 116×116 matrix based on white matter fiber numbers between paired ROIs for each subject.

2.2 Proposed Method

Our goal is to model region-specific and inter-region dependencies between dynamic FC and SC graphs (from fMRI and DTI, respectively) for neurocognitive decline analysis. As shown in Fig. 1, the proposed DFSC consists of (1) modality-specific graph embedding learning, (2) dynamic function-structure connectivity (FSC) coupling learning, and (3) multi-view feature fusion and prediction.

Modality-Specific Graph Embedding Learning. Resting-state fMRI helps reveal functional interactions between ROIs based on synchronized brain neural activity, while DTI reflects brain physical connections by quantifying between-region white matter fibers [8]. To explore brain connectivity patterns from physiological and anatomical views, we construct an FC graph from fMRI and an SC graph from DTI for each subject. Considering that fMRI time series fluctuate over time, we use sliding windows to divide regional signals into T segments and compute Pearson correlation between paired ROIs within each segment, yielding dynamic FC matrices $X_t^F \in \mathbb{R}^{N \times N}$ $(t{=}1, \cdots, T)$. For DTI, we normalize the preprocessed white fiber number matrix, obtaining an SC matrix $X^S \in \mathbb{R}^{N \times N}$, where $N{=}116$ is the number of ROIs. To remove redundant and noisy information in brain networks [21, 31], we keep the top 30% strongest connectivities to generate $T+1$ adjacency matrices (*i.e.*, $\{A_t^F\}_{t=1}^T$ and A^S) for FC and SC graphs.

With the constructed graphs as input for each modality, we use the graph attention network (GAT) [29] as the backbone to learn graph embeddings by aggregating node features from their neighbors. The updated node embedding is formulated as: $E=\sigma\left(\sum_{k=1}^{K} A^k X W^k\right) \in \mathbb{R}^{N\times D}$, where σ is an activation function, K is the number of attention heads, W^k is the learnable weight matrix, and D is the dimension of learned embedding. The to-be-learned connection weight between the ROIs i and j in A^k at the k-th self-attention head is formulated as:

$$a_{ij} = \frac{\exp\left(\psi\left[x_i W \| x_j W\right]\eta^T\right)}{\sum_{j'\in\mathcal{N}_i}\exp\left(\psi\left[x_i W \| x_{j'} W\right]\eta^T\right)}, \tag{1}$$

where ψ is the LeakyReLU function, x_i and x_j are node features for ROI i and j, $\|$ denotes concatenation, η is a learnable weight vector, W is the trainable weight matrix, and $\mathcal{N}_i$ is the neighboring node set for ROI i. The self-attention mechanism in Eq. (1) computes attention scores for each node to its neighbors, thereby assigning importance weights to each neighbor's features for updating its own representation and extracting informative graph embeddings. With a multi-branch GAT architecture (see Fig. 1), we obtain dynamic FC embeddings $E_t^F \in \mathbb{R}^{N\times D}$ $(t{=}1,\cdots,T)$ and SC embedding $E^S \in \mathbb{R}^{N\times D}$ for each subject.

Dynamic FSC Coupling Learning. Previous evidence suggests that alterations in FSC coupling are associated with neurocognitive decline [14]. Different from existing studies that mainly investigate the interplay between static FC and SC features [14,26], we explore how the interactions between FC and SC change over time based on dynamic FC and SC embeddings. For each time segment t, we calculate the Pearson correlation between the learned FC embedding E_t^F and SC feature E^S to construct an *FSC coupling graph* with the adjacency matrix A_t^{FS}, where the coupling strength a_{ij}^{FS} between ROIs i and j is defined as:

$$a_{ij}^{FS} = \frac{\sum_{k=1}^{D}\left(E_t^F(i,k)-\bar{E}_t^F(i)\right)\left(E^S(j,k)-\bar{E}^S(j)\right)}{\sqrt{\sum_{k=1}^{D}\left(E_t^F(i,k)-\bar{E}_t^F(i)\right)^2\sum_{k=1}^{D}\left(E^S(j,k)-\bar{E}^S(j)\right)^2}}, \tag{2}$$

where $E_t^F(i,k)$ and $E^S(j,k)$ are the k-th feature of the i-th row in FC embedding and the j-th row in SC embedding, and $\bar{E}_t^F(i)$ and $\bar{E}^S(i)$ are the mean values of the i-th row of FC embedding and the j-th row of SC embedding. Unlike conventional FSC coupling focusing on region-specific interactions between FC and SC [26], our coupling graph can *simultaneously model region-specific and inter-region dependencies* between FC and SC patterns, providing a *fine-grained profile of dynamic interplay* between physiological and anatomical connectivity. For the FSC coupling graph at segment t, we use coupling strength as node feature, with the node feature matrix represented as $X_t^{FS}{=}A_t^{FS}$.With dynamic FSC coupling graphs $\{G_t^{FS}{=}(A_t^{FS},X_t^{FS})\}_{t=1}^T$ as input, we adopt multi-branch GATs for feature learning, producing dynamic FSC coupling embeddings $\{E_t^{FS}\}_{t=1}^T \in \mathbb{R}^{N\times D}$.

Multi-View Feature Fusion & Prediction. With multi-view dynamic graph embeddings ($\{E_t^F\}_{t=1}^T$, E^S, and $\{E_t^{FS}\}_{t=1}^T$) as input, we use squeeze-excitation

Table 1. Results of different methods in 2 tasks. The term '*' denotes that the results of DFSC and a competing method are statistically significantly different ($p < 0.05$).

Method	SMC vs. NC classification on ADNI					ANI vs. NC classification on HCD				
	AUC (%)	ACC (%)	SEN (%)	SPE (%)	BAC (%)	AUC (%)	ACC (%)	SEN (%)	SPE (%)	BAC (%)
SVM	59.2(8.8)*	55.3(5.2)	59.5(6.8)	51.8(9.1)	55.6(6.1)	59.4(2.2)*	54.4(1.7)	55.7(3.6)	52.3(4.1)	53.9(1.3)
RF	57.9(4.5)*	56.3(3.8)	59.0(6.1)	56.3(3.8)	57.7(3.3)	55.1(5.2)*	52.9(4.0)	52.9(6.5)	54.6(4.2)	53.7(3.9)
GCN	63.1(4.9)*	57.6(3.6)	62.5(1.2)	54.7(6.0)	58.6(3.0)	64.2(2.1)*	59.6(2.3)	58.7(5.1)	61.7(4.9)	60.2(2.4)
GAT	65.6(4.5)*	58.5(2.3)	**65.7(8.3)**	52.9(9.7)	59.3(1.7)	65.7(3.9)	61.1(3.0)	62.5(5.8)	59.5(6.0)	61.0(0.1)
BrainNetCNN	64.7(9.3)*	60.1(6.7)	58.2(3.2)	62.3(14.2)	60.2(8.7)	62.4(2.6)*	58.8(1.3)	58.2(6.0)	60.6(3.1)	59.4(1.9)
BrainGNN	63.9(4.2)*	60.3(3.4)	62.2(3.8)	57.5(7.7)	59.9(2.2)	63.0(3.2)*	60.3(2.6)	56.3(6.0)	63.7(5.6)	60.0(1.8)
STAGIN	65.0(5.4)*	58.5(6.3)	59.6(5.5)	60.2(9.6)	59.9(5.6)	63.7(4.0)*	60.6(2.6)	62.0(3.2)	60.8(1.7)	61.4(2.4)
HGNN	66.5(5.1)*	60.4(5.5)	64.1(6.5)	57.8(5.9)	60.9(5.8)	66.9(1.9)*	59.5(2.3)	58.1(2.6)	63.2(3.7)	60.6(2.6)
M-GCN	58.5(7.4)*	53.4(4.7)	54.3(12.1)	53.2(8.3)	53.8(4.6)	54.3(7.2)*	52.7(4.9)	53.6(12.7)	53.6(11.7)	53.6(5.3)
Cross-GNN	68.8(6.7)*	59.8(6.5)	62.1(8.0)	61.5(7.6)	61.8(6.5)	60.7(4.4)*	57.3(4.4)	**62.9(7.0)**	54.8(5.2)	58.8(4.1)
DFSC (Ours)	**70.7(3.6)**	**63.5(4.0)**	59.8(7.5)	**69.2(4.2)**	**64.5(3.4)**	**68.2(3.1)**	**62.1(2.6)**	61.3(1.8)	**64.2(3.9)**	**62.7(2.3)**

(SE) [17] to convert node-level embeddings to graph-level features, formulated as $f{=}E\Phi(P_2\sigma(P_1E\phi_{mean}))$, where Φ is a sigmoid function, P_1 and P_2 are learnable weight matrices in a multilayer perceptron (MLP), σ is an activation function, and ϕ_{mean} is an average operation. In this way, one can identify contributions of each ROI to downstream tasks. With SE-based readout, we get multi-view features $\{f_t^F\}_{t=1}^T$, f^S, and $\{f_t^{FS}\}_{t=1}^T$, followed by a single-head Transformer [32] for feature fusion. Specifically, we first stack the multi-view features to form an input matrix $F{=}[f_1^F, \cdots, f_T^F, f^S, f_1^{FS}, \cdots, f_T^{FS}]^\top \in \mathbb{R}^{(2T+1)\times D}$. Denoting φ_1, φ_2, and φ_3 as linear operations, the self-attention matrix across dynamic FC, SC, and FSC coupling features is computed as $Z{=}\text{Softmax}\left(QK^\top/\sqrt{d}\right)$, where $Q{=}\varphi_1(F)$, $K{=}\varphi_2(F)$, and d is a scaling factor. So we can obtain temporally and cross-view attended feature via $\tilde{F}{=}ZV{=}Z\varphi_3(F)\in \mathbb{R}^{(2T+1)\times D}$. This helps capture *long-range dependencies across time segments and multiple views*, enhancing discriminative power of learned features. We then average the attended feature $\tilde{F}$ to generate a D-dimensional feature vector for each subject, followed by an MLP for prediction.

The DFSC provides a data-driven framework for modeling temporally dynamic interactions between FC and SC patterns. It is implemented in PyTorch and trained using an Adam optimizer with a cross-entropy loss (learning rate: 10^{-5}, batch size: 12, epoch: 30). The time segments (T) are 6, the graph embedding dimension (D) is 64, and attention heads (K) in GAT are 4.

3 Experiment

Experimental Settings. DFSC is compared with 10 approaches: two traditional methods (*i.e.*, **SVM** [16] and **RF** [3]) with 1,168-dimensional node-level and graph-level features from FC and SC graphs; two popular graph learning methods with fMRI (*i.e.*, **GCN** [22] and **GAT** [29]); two SOTA methods specifically designed for fMRI-based brain network analysis (*i.e.*, **BrainNetCNN** [19] and **BrainGNN** [25]); one method that considers temporal dynamics in fMRI (*i.e.*, **STAGIN** [21]); and three SOTA methods for multi-modal graph fusion (*i.e.*, **HGNN** [13], **M-GCN** [8] and **Cross-GNN** [35]). We use default configurations of competing methods [12] and diligently ensure their training hyperparameters are comparable to ours. Five-fold cross-validation is utilized. Several metrics are used: area under ROC curve (AUC), accuracy (ACC), sensitivity

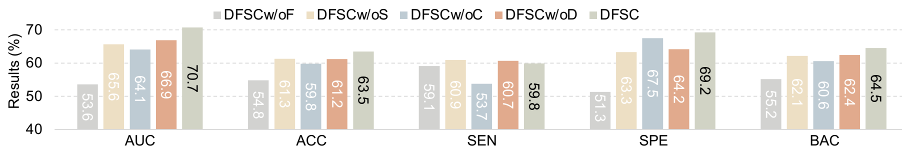

Fig. 2. Results (%) of our method and its variants in SMC vs. NC classification.

Table 2. Results (%) of the proposed DFSC using different FSC coupling strategies.

Method	AUC (%)	ACC (%)	SEN (%)	SPE (%)	BAC (%)	p-value
DFSC_CS	65.3(2.4)	59.9(3.1)	58.2(5.6)	62.7(7.5)	60.4(2.5)	0.0016
DFSC_SR	67.4(2.7)	60.3(2.3)	57.2(8.9)	65.8(5.2)	61.5(2.4)	0.0331
DFSC	**70.7(3.6)**	**63.5(4.0)**	**59.8(7.5)**	**69.2(4.2)**	**64.5(3.4)**	–

(SEN), specificity (SPE), and balanced accuracy (BAC). A paired t-test is used to assess significant differences between DFSC and each competing method.

Results. Table 1 reports the results achieved by 10 competing methods and our DFSC on ADNI and HCD datasets. From Table 1, we can observe that the DFSC outperforms two traditional methods (*i.e.*, SVM and RF) that rely on hand-crafted features by a large margin. Besides, our DFSC generally yields superior performance over two popular graph learning methods (*i.e.*, GCN and GAT) and three SOTA models (*i.e.*, BrainNetCNN, BrainGNN, and STAGIN) that only leverage single-modality information. This demonstrates the effectiveness of integrating multi-modal brain networks for neurocognitive decline analysis. Compared with two SOTA multi-modal methods (*i.e.*, HGNN and M-GCN), which do not consider interactions between FC and SC patterns, our DFSC produces better classification performance. The possible reason is that our DFSC can capture dynamic cross-modality dependencies while leveraging multi-view complementary features derived from FC, SC, and FSC graphs for prediction. In particular, Cross-GNN, which also considers inter-modality relationships (as we do in DFSC), performs worse than DFSC in most cases. The possible reason is that Cross-GNN fails to capture temporal variations conveyed in time series data of fMRI, while our DFSC explicitly models such temporal dynamics.

Ablation Study. We compare the DFSC with its four degenerated variants: 1) **DFSCw/oF** that only uses SC from DTI, 2) **DFSCw/oS** that only uses FC from fMRI, 3) **DFSCw/oC** that directly integrates learned FC and SC embeddings, without explicitly modeling FSC coupling graphs, and 4) **DFSCw/oD** without considering temporal dynamics in fMRI. Results of the five methods in SMC vs. NC classification are shown in Fig. 2. As can be seen in Fig. 2, DFSC is superior to its two single-modality variants (*i.e.*, DFSCw/oF and DFSCw/oS), verifying the necessity of utilizing multi-modality information. Besides, DFSC outperforms DFSCw/oC that ignores interactions between FC and SC features. This implies that modeling FSC coupling graphs can provide a complementary view for enhanced prediction performance. Moreover, DFSCw/oD is inferior to

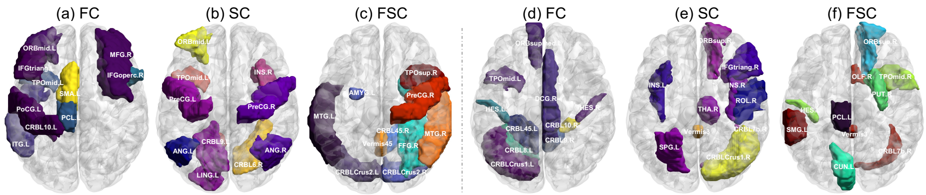

Fig. 3. Visualization of top 10 discriminative ROIs identified by our method from FC, SC, and FSC graphs in (a-c) SMC vs. NC and (d-f) ANI vs. NC classification.

DFSC in most cases, indicating that capturing temporal dynamics in FC and FSC graphs helps improve the discriminative power of learned embeddings.

Influence of FSC Coupling Strategy. In DFSC, we calculate Pearson correlation (PC) between learned FC and SC embedding to construct FSC coupling graphs. We also explore cosine similarity (CS) and Spearman's rank (SR) correlation to measure FSC coupling strength and denote the two methods as **DFSC_CS** and **DFSC_SR** respectively. Table 2 shows the results in SMC vs. NC classification, from which we see that our DFSC using PC outperforms its two variants. The likely reason is that PC better captures FSC coupling magnitude, while CS measures angular similarity and SR focuses on rank-based relations.

Identified Discriminative Regions. Based on learned FC, SC and FSC graph embeddings, we use the squeeze-excitation (SE) strategy [17] to automatically identify contributions of ROIs to the final prediction. We visualize the top 10 discriminative ROIs identified by DSFC from FC, SC, and FSC graphs for SMC vs. NC classification in Fig. 3 (a-c) and ANI vs. NC classification in Fig. 3 (d-f).

For SMC vs. NC classification, Fig. 3 (a-c) shows that the discriminative ROIs located in the *temporal pole* are consistently detected across FC, SC, and FSC graphs, consistent with prior research linking it to immediate recall performance [33]. Notably, several important ROIs are highlighted in the FSC coupling graph, such as *amygdala* and *middle temporal gyrus*, which have been proven to be associated with SMC [7, 23]. Specifically, the amygdala is highly involved in emotional regulation and memory modulation and middle temporal gyrus plays a role in semantic and verbal memory [7]. Their abnormalities may contribute to cognitive and memory concerns observed in SMC patients.

Fig. 3 (d-f) shows that, for ANI vs. NC classification, several cerebellar regions (*e.g.*, *cerebellar lobule* and *cerebellar vermis*) are consistently identified from FC, SC, and FSC graphs, implying HIV infection can trigger cerebellum-related dysfunction early, affecting cognition and motor functions for ANI patients [30]. From SC graphs, one can identify the abnormality in *thalamus*, aligning with prior knowledge that HIV patients exhibit structural atrophy in thalamus, even when achieving viral suppression under cART treatment [28]. *Superior frontal gyrus* is consistently detected from FC, SC, and FSC graphs. Previous research also suggests that HIV infection causes neuronal loss in the frontal cor-

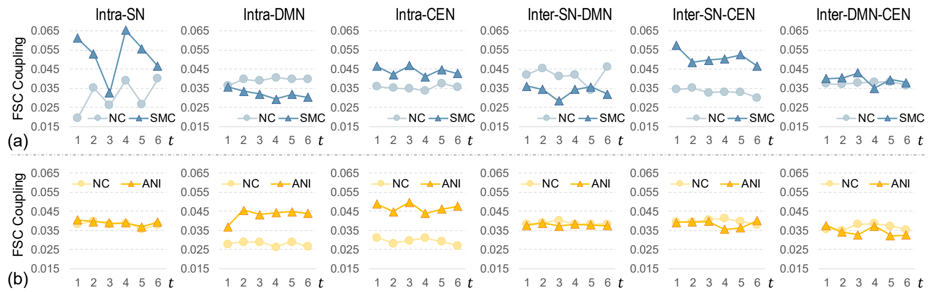

Fig. 4. Dynamic FSC coupling strength difference among SN, DMN, and CEN modules with T=6 segments in (a) SMC vs. NC classification and (b) ANI vs. NC classification.

tex and induces adaptive synaptic changes [10]. These changes may affect the prefrontal-striatal circuit, leading to executive dysfunction in ANI patients [9].

Between-Group FSC Coupling Difference. Our DFSC can model FSC coupling matrices across T time segments. To quantitatively analyze dynamic FSC coupling difference between patient and NC groups, we perform group-level statistical analysis to identify significant FSC couplings. For each group, we calculate intra- and inter-module coupling strength across 3 prominent resting-state neurocognitive modules, *i.e.*, salience network (SN), default mode network (DMN), and central executive network (CEN), with results reported in Fig. 4. Fig. 4 (a) suggests that the overall FSC coupling strength across T segments within DMN is reduced for SMC patients. This matches prior findings that early cognitive impairment disrupts connections within DMN [36]. Additionally, the between-group coupling difference for inter-SN-DMN and inter-SN-CEN connections is more significant than that for inter-DMN-CEN connection, implying SMC patients exhibit abnormal SN function in mapping external stimuli and internal mental events [24]. Fig. 4 (b) shows that ANI patients exhibit decreased inter-module connection between SN and CEN. This could be linked to impairments in executive function and attention in HIV-infected patients [4]. We also observe SMC and ANI patients show increased FSC coupling strength within CEN than NCs. Higher FSC coupling may reflect a compensatory mechanism in the brain that helps prevent early neurocognitive decline, as proven by [1].

4 Conclusion

This paper presents a dynamic function-structure connectivity coupling (DFSC) framework for neurocognitive decline analysis. Leveraging fMRI and DTI data, DFSC first extracts modality-specific graph embeddings from fMRI and DTI, and then learns dynamic FSC coupling graph embeddings, followed by multi-view feature fusion for prediction. Notably, our FSC coupling graph considers temporal dynamics in fMRI while modeling both region-specific and inter-region dependencies between FC and SC patterns, providing a fine-grained profile of the interplay between brain function and structure. Extensive experiments on two cohorts demonstrate the superiority of DFSC over state-of-the-art methods. DFSC can identify discriminative brain regions and quantify between-group FSC coupling differences, providing potential biomarkers for early detection. In the future, we will extend the DFSC to model long-term FSC coupling changes using longitudinal data for graph-based cognitive decline analysis. Additionally, we plan to employ advanced domain adaptation techniques [11, 15] to address the potential issue of small data, thereby improving model robustness.

Acknowledgments. Q. Wang and W. Wang contribute equally to this work.

Disclosure of Interests. The authors have no competing interests to declare that are relevant to the content of this article.

References

1. Barulli, D., Stern, Y.: Efficiency, capacity, compensation, maintenance, plasticity: emerging concepts in cognitive reserve. Trends in Cognitive Sciences **17**(10), 502–509 (2013)
2. Baum, G.L., Cui, Z., Roalf, D.R., Ciric, R., Betzel, R.F., Larsen, B., Cieslak, M., Cook, P.A., Xia, C.H., Moore, T.M., et al.: Development of structure–function coupling in human brain networks during youth. PNAS **117**(1), 771–778 (2020)
3. Breiman, L.: Random Forests. Machine Learning **45**, 5–32 (2001)
4. Chaganti, J., Heinecke, A., Gates, T., Moffat, K., Brew, B.: Functional connectivity in virally suppressed patients with HIV-associated neurocognitive disorder: A resting-state analysis. American Journal of Neuroradiology **38**(8), 1623–1629 (2017)
5. Collin, G., Scholtens, L.H., Kahn, R.S., Hillegers, M.H., van den Heuvel, M.P.: Affected anatomical rich club and structural–functional coupling in young offspring of schizophrenia and bipolar disorder patients. Biological Psychiatry **82**(10), 746–755 (2017)
6. Cui, Z., Zhong, S., Xu, P., He, Y., Gong, G.: PANDA: a pipeline toolbox for analyzing brain diffusion images. Frontiers in Human Neuroscience **7**, 42 (2013)
7. Dong, Q.Y., Li, T.R., Jiang, X.Y., Wang, X.N., Han, Y., Jiang, J.H.: Glucose metabolism in the right middle temporal gyrus could be a potential biomarker for subjective cognitive decline: a study of a Han population. Alzheimer's Rresearch & Therapy **13**, 1–12 (2021)
8. Dsouza, N.S., Nebel, M.B., Crocetti, D., Robinson, J., Mostofsky, S., Venkataraman, A.: M-GCN: A multimodal graph convolutional network to integrate functional and structural connectomics data to predict multidimensional phenotypic characterizations. In: Medical Imaging with Deep Learning. pp. 119–130. PMLR (2021)
9. Du Plessis, S., Vink, M., Joska, J.A., Koutsilieri, E., Stein, D.J., Emsley, R.: HIV infection and the fronto–striatal system: A systematic review and meta-analysis of fMRI studies. AIDS **28**(6), 803–811 (2014)
10. Everall, I., Luthert, P., Lantos, P.: Neuronal loss in the frontal cortex in HIV infection. The Lancet **337**(8750), 1119–1121 (1991)

11. Fang, Y., Yap, P.T., Lin, W., Zhu, H., Liu, M.: Source-free unsupervised domain adaptation: A survey. Neural Networks p. 106230 (2024)
12. Fang, Y., Zhang, J., Wang, L., Wang, Q., Liu, M.: ACTION: Augmentation and computation toolbox for brain network analysis with functional MRI. NeuroImage **305**, 120967 (2025)
13. Feng, Y., You, H., Zhang, Z., Ji, R., Gao, Y.: Hypergraph neural networks. In: Proceedings of the AAAI Conference on Artificial Intelligence. vol. 33, pp. 3558–3565 (2019)
14. Gu, Z., Jamison, K.W., Sabuncu, M.R., Kuceyeski, A.: Heritability and interindividual variability of regional structure-function coupling. Nature Communications **12**(1), 4894 (2021)
15. Guan, H., Liu, M.: DomainATM: Domain Adaptation Toolbox for Medical Data Analysis. NeuroImage p. 119863 (2023)
16. Hearst, M.A., Dumais, S.T., Osuna, E., Platt, J., Scholkopf, B.: Support vector machines. IEEE Intelligent Systems and Their Applications **13**(4), 18–28 (1998)
17. Hu, J., Shen, L., Sun, G.: Squeeze-and-excitation networks. In: CVPR. pp. 7132–7141 (2018)
18. Jack Jr, C.R., Bernstein, M.A., Fox, N.C., Thompson, P., Alexander, G., Harvey, D., Borowski, B., Britson, P.J., L. Whitwell, J., Ward, C., et al.: The Alzheimer's disease neuroimaging initiative (ADNI): MRI methods. Journal of Magnetic Resonance Imaging: An Official Journal of the International Society for Magnetic Resonance in Medicine **27**(4), 685–691 (2008)
19. Kawahara, J., Brown, C.J., Miller, S.P., Booth, B.G., Chau, V., Grunau, R.E., Zwicker, J.G., Hamarneh, G.: BrainNetCNN: Convolutional neural networks for brain networks; towards predicting neurodevelopment. NeuroImage **146**, 1038–1049 (2017)
20. Kesler, S.R., Adams, M., Packer, M., Rao, V., Henneghan, A.M., Blayney, D.W., Palesh, O.: Disrupted brain network functional dynamics and hyper-correlation of structural and functional connectome topology in patients with breast cancer prior to treatment. Brain and Behavior **7**(3), e00643 (2017)
21. Kim, B.H., Ye, J.C., Kim, J.J.: Learning dynamic graph representation of brain connectome with spatio-temporal attention. NeurIPS **34**, 4314–4327 (2021)
22. Kipf, T.N., Welling, M.: Semi-supervised classification with graph convolutional networks. arXiv preprint arXiv:1609.02907 (2016)
23. Kuhn, E., Perrotin, A., Tomadesso, C., André, C., Sherif, S., Bejanin, A., Touron, E., Landeau, B., Mezenge, F., Vivien, D., et al.: Subjective cognitive decline: opposite links to neurodegeneration across the Alzheimer's continuum. Brain Communications **3**(3), fcab199 (2021)
24. Li, C., Li, Y., Zheng, L., Zhu, X., Shao, B., Fan, G., Liu, T., Wang, J., Alzheimer's Disease Neuroimaging Initiative: Abnormal brain network connectivity in a triple-network model of Alzheimer's disease. Journal of Alzheimer's Disease **69**(1), 237–252 (2019)
25. Li, X., Zhou, Y., Dvornek, N., Zhang, M., Gao, S., Zhuang, J., Scheinost, D., Staib, L.H., Ventola, P., Duncan, J.S.: BrainGNN: Interpretable brain graph neural network for fMRI analysis. Medical Image Analysis **74**, 102233 (2021)
26. Li, Y., Wei, Q., Adeli, E., Pohl, K.M., Zhao, Q.: Joint graph convolution for analyzing brain structural and functional connectome. In: MICCAI. pp. 231–240. Springer (2022)
27. Markello, R.D., Hansen, J.Y., Liu, Z.Q., Bazinet, V., Shafiei, G., Suárez, L.E., Blostein, N., Seidlitz, J., Baillet, S., Satterthwaite, T.D., et al.: Neuromaps: struc-

tural and functional interpretation of brain maps. Nature Methods **19**(11), 1472–1479 (2022)
28. Nichols, M.J., Gates, T.M., Soares, J.R., Moffat, K.J., Rae, C.D., Brew, B.J., Cysique, L.A.: Atrophic brain signatures of mild forms of neurocognitive impairment in virally suppressed HIV infection. AIDS **33**(1), 55–66 (2019)
29. Veličković, P., Cucurull, G., Casanova, A., Romero, A., Lio, P., Bengio, Y.: Graph Attention Networks. arXiv preprint arXiv:1710.10903 (2017)
30. Wächter, C., Eiden, L.E., Naumann, N., Depboylu, C., Weihe, E.: Loss of cerebellar neurons in the progression of lentiviral disease: effects of CNS-permeant antiretroviral therapy. Journal of Neuroinflammation **13**, 1–13 (2016)
31. Wang, Q., Wang, W., Fang, Y., Yap, P.T., Zhu, H., Li, H.J., Qiao, L., Liu, M.: Leveraging brain modularity prior for interpretable representation learning of fMRI. IEEE Transactions on Biomedical Engineering **71**(8), 2391–2401 (2024)
32. Waswani, A., Shazeer, N., Parmar, N., Uszkoreit, J., Jones, L., Gomez, A., Kaiser, L., Polosukhin, I.: Attention is all you need. In: NeurIPS (2017)
33. Wolk, D.A., Dickerson, B.C., Initiative, A.D.N., et al.: Fractionating verbal episodic memory in Alzheimer's disease. NeuroImage **54**(2), 1530–1539 (2011)
34. Yan, C., Zang, Y.: DPARSF: A MATLAB toolbox for "pipeline" data analysis of resting-state fMRI. Frontiers in Systems Neuroscience **4**, 13 (2010)
35. Yang, Y., Ye, C., Guo, X., Wu, T., Xiang, Y., Ma, T.: Mapping multi-modal brain connectome for brain disorder diagnosis via cross-modal mutual learning. IEEE Transactions on Medical Imaging **43**, 108–121 (2023)
36. Zhan, Y., Ma, J., Alexander-Bloch, A.F., Xu, K., Cui, Y., Feng, Q., Jiang, T., Liu, Y., Initiative, A.D.N., et al.: Longitudinal study of impaired intra-and internetwork brain connectivity in subjects at high risk for Alzheimer's disease. Journal of Alzheimer's Disease **52**(3), 913–927 (2016)